# Adsorption of Pt and Bimetallic PtAu Clusters on the Partially Reduced Rutile (110) TiO$_2$ Surface: A First-Principles Study

D. Çakır[†] and O. Gülseren*

Department of Physics, Bilkent University, 06800 Ankara, Turkey

ABSTRACT: An extensive study of the adsorption of small Pt$_n$ (n = 1−8) and bimetallic Pt$_2$Au$_m$ (m = 1−5) clusters on the partially reduced rutile (110) TiO$_2$ surface has been performed via total energy pseudopotential calculations based on density functional theory. Structures, energetics, and electronic properties of adsorbed Pt$_n$ and Pt$_2$Au$_m$ clusters have been determined. The surface oxygen vacancy site has been found to be the nucleation center for the growth of Pt clusters. These small Pt clusters strongly interact with the partially reduced surface and prefer to form planar structures for n = 1−6 since the cluster−substrate interaction governs the cluster growth at low Pt coverage. We found a planar-to-three-dimensional structural transition at n = 7 for the formation of Pt$_n$ clusters on the reduced TiO$_2$ surface. GGA+U calculations have also been performed to get a reasonable description of the reduced oxide surface. We observed significant band gap narrowing upon surface−Pt$_n$ cluster interaction which leads to the formation of gap localized Pt states. In the case of bimetallic Pt−Au clusters, Au$_m$ clusters have been grown on the Pt$_2$−TiO$_2$ surface. The previously adsorbed Pt dimer at the vacancy site of the reduced surface acts as a clustering center for Au atoms. The presence of the Pt dimer remarkably enhances the binding energy and limits the migration of Au atoms on the titania surface. The charge state of both individual atoms and clusters has been obtained from the Bader charge analysis, and it has been found that charge transfer among the Pt atoms of Pt$_n$ clusters and the metal oxide surface is stronger compared to that of Au clusters and the Pt$_2$−TiO$_2$ system.
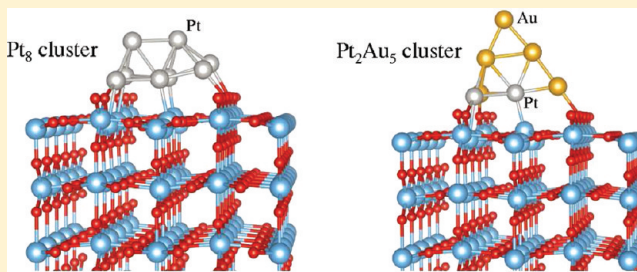
INTRODUCTION

TiO$_2$ is a versatile material and extensively used as both catalysts and catalyst supports due to its several advantages including high activity, low cost, chemical and mechanical stabilities in different conditions, environmental compatibility, and stability under illumination. Pt−TiO$_2$ and Au−TiO$_2$ are the most active systems studied both theoretically and experimentally.[1−18] Au nanoparticles supported on the TiO$_2$ surfaces exhibit unusual catalytic activity for CO oxidation at low temperatures,[2,19−21] while the bulk form of Au is known as a chemically inert material. Similarly, Pt−TiO$_2$ is considered as the prototype of strong-metal−support-interaction (SMSI)[1,22] which is a strong interaction observed between the small metal clusters and TiO$_2$ surface and influences the catalytic activity over the surface.

Surface defects such as oxygen vacancies are generally believed to play an important role in the growth of metal clusters. Metal adatoms can be easily trapped in the defect sites. These defect sites behave as nucleation centers for the adatoms diffusing on the surface. Furthermore, it is contemplated that O vacancies influence the catalysis over the metal oxide surfaces. There are several studies reporting that small gold clusters adsorbed on an oxygen vacancy of the TiO$_2$ surface become negatively charged, and this charging causes the unusual catalytic activity of this small Au cluster.[15,23−25]

Because of the important scientific and technological applications of Pt− and Au−TiO$_2$ systems, a fundamental study of the interaction between these metal atoms and defect-free as well as partially reduced rutile (110) surface is crucial, and it will contribute to our understanding about photocatalytic applications of TiO$_2$ surfaces. In this study, we have presented a complete picture for the interaction of Pt and bimetallic PtAu clusters with the partially reduced TiO$_2$ surface within density functional theory. The growth behaviors of such small clusters help to get more insight into the early stage nucleation of the Pt and bimetallic Pt−Au nanoparticles dispersed on the titania surfaces. Bimetallic PtAu clusters adsorbed on the TiO$_2$ surfaces promise a great potential to produce special catalysts which have high activity, selectivity, and stability in photocatalysis through tuning of their compositions. We believe that our results are crucial for further research on these metal−titania systems to reveal their properties for practical applications.

RESULTS AND DISCUSSIONS

We have carried out the plane-wave calculations[26,27] within density functional theory (DFT)[28] for the first-principles investigation of Pt and bimetallic PtAu clusters on the partially reduced rutile (110) TiO$_2$ surfaces. We have used projector augmented-wave (PAW) potentials[29,30] to describe the ions within the pseudopotential approximation. The exchange-
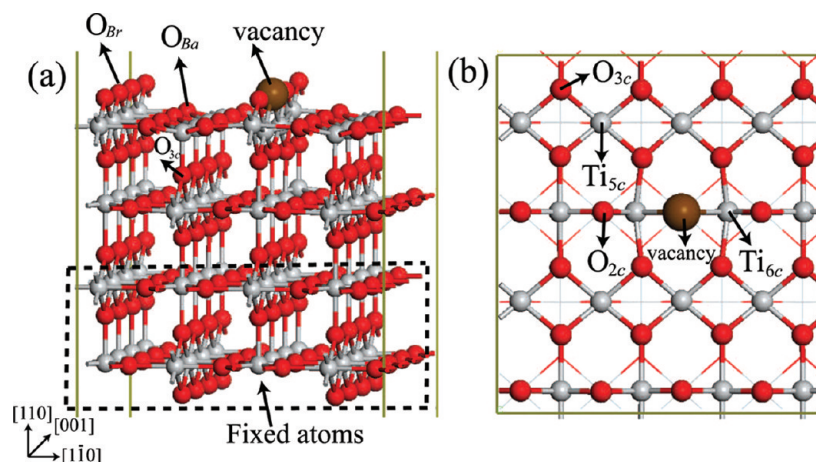
Figure 1. Side (a) and top (b) views of the partially reduced 4 × 2 rutile (110) surface. Position of the O vacancy is displayed by a large ball (brown color). Light (gray) and dark (red) colors represent Ti and O atoms, respectively. The coordination of some of the atoms is indicated as subscripts. O_{Br}, O_{Ba}, and O_{3c} represent the 2-fold coordinated surface bridge and 3-fold coordinated surface basal and 3-fold coordinated bulk oxygen atoms, respectively. O and Ti atoms within the dashed rectangular region do not allow movement (frozen) during the relaxation calculations to simulate the bulk part.

correlation contributions have been treated using the generalized gradient approximation (GGA) with PW91 formulation.[31] The rutile (110) surface has been modeled by a 4 × 2 surface unit cell by constructing a slab geometry. The vacuum region between the periodic images has been taken at least 9 Å. Due to the large supercell, Γ point has been used for the Brillouin zone sampling. A plane-wave basis set with kinetic energy cutoff of 500 eV has been taken. The convergence has been achieved when the difference of the total energies between two consecutive ionic steps has been less than 10^{-5} eV and the maximum force allowed on each atom has been 0.02 eV/Å. To treat partial occupancies of the bands, the Gaussian smearing method[32] has been used, and the width of smearing has been chosen as 0.05 eV. For the density of states calculations (DOS), a finer k-mesh has been used within the Monkhorst–Pack scheme.[33] In this study, the partially reduced rutile (110) surface has been modeled by a four-layer thick slab, in which the two bottom layers have been kept at bulk positions.[34] As discussed in detail by Hameeuw et al.,[34] using two bottom layers fixed at their bulk positions is very crucial both for correct physical representation and for convergence of physical quantities with respect to the slab thickness. According to our tests as well as the previous calculations on the same surface systems,[7,8,10] a four-layer slab (i.e., 4 O–Ti₂O₂–O trilayers and hence 12 atomic layers) can be considered as the smallest representation of the rutile (110) surface. We have used this slab model in the calculations unless otherwise stated. The surface energy of the rutile (110) surface within the current computational setup is found to be 0.50 J/m² which is fairly close to converged surface energy value of 0.58 (0.47) J/m² computed by using the PW91 (PBE) functional in ref 35. Furthermore, displacements of the surface atoms of the stoichiometric surface listed as 0.05 Å (0.08 ± 0.05 Å) for bridging O (O_{Br}), 0.18 Å (0.19 ± 0.08 Å) for surface O (O_{Ba}), 0.25 Å (0.24 ± 0.03 Å) for 6-fold coordinated Ti (Ti_{6c}), and −0.14 Å (−0.19 ± 0.03 Å) for 5-fold coordinated Ti (Ti_{5c}) (while the positive displacement means upward, the negative sign shows downward displacement) are compared very well with the corresponding experimental LEED values[36] quoted in parentheses. Lattice parameters *a* and *c* of rutile calculated within GGA are 4.64 (4.59) and 2.97 (2.96) Å, respectively.

These results are in good agreement with the experimental values[37–39] which are quoted in parentheses. The chosen parameters have been proven to be sufficient for describing the Pt and bimetallic Pt Au–TiO₂ systems.

When a bridge oxygen atom is removed from the rutile TiO₂(110) surface, two unpaired electrons are left on the system. There is a debate about the correct description of these excess charges in the literature. According to some experimental studies, the reduction of the titania surface produces Ti³⁺ ions and localized gap states originating from Ti 3d states.[1] On the other hand, Krüger et al., from resonant photoelectron diffraction experiments, reported that the defect charges are distributed over several surface and subsurface Ti sites at finite temperature.[40] Nonetheless, standard DFT calculations using either GGA or LDA on the reduced rutile (110) surface predict delocalization of the excess charge over several Ti sites in the surface and subsurface layers and give metallic character and have failed to reproduce experimentally observed electronic structure[41] because of the improper description of strongly correlated 3d electrons localized on Ti atoms. Moreover, Kowalski et al. showed that the excess charge localized on Ti sites migrates easily to other Ti sites by the help of phonon-assisted hopping, leading to an effective delocalization on the average.[42] Furthermore, the excess charge populates the various local minima of similar energies but different topologies because of the thermal fluctuations. Besides, Deskins et al. denoted that the electron transport in bulk TiO₂ proceeds via thermal hopping of electron polarons among the low-energy Ti sites with activation energies on the order of ~0.1 eV.[43–45] Localized and delocalized states are very close in energy and can depend on external conditions like temperature. From DFT calculations, only hybrid[46] or DFT+U[47] functionals result in localized states. We have also performed GGA+U[48] calculations in addition to the GGA ones to make comparison between two different functionals. Especially, we have considered the GGA+U to investigate the electronic properties. The value of U is critical; if $3.0 \leq U \leq 6.0$ eV, both electrons are localized on different Ti atoms.[49] Also, a self-consistent Hubbard U correction as 3.4 eV for the d electrons of the rutile Ti atoms has been calculated by using the linear response approach.[50] Likewise, Morgan et al.[47] used a U value of 4.2 eV to reproduce
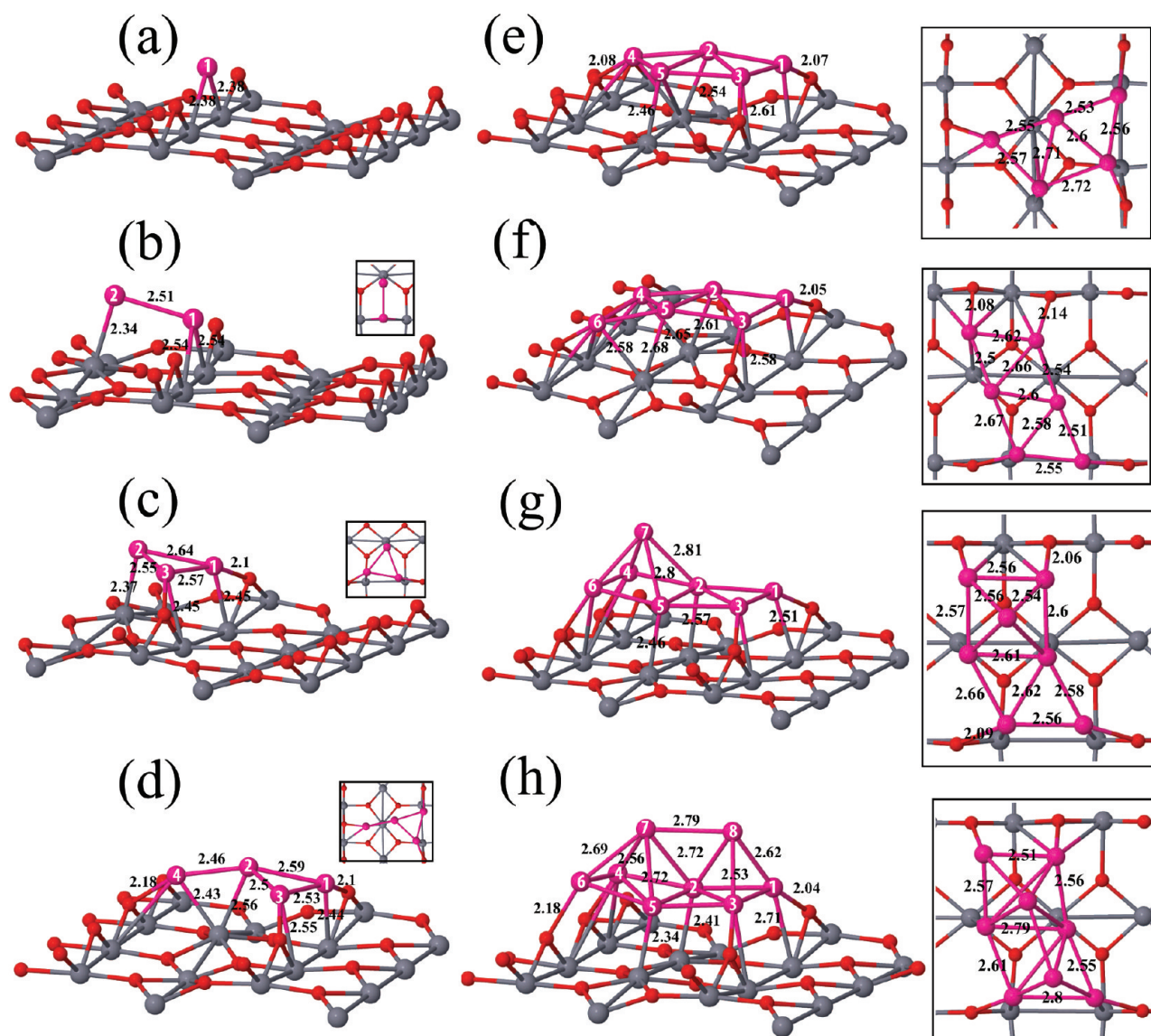
Figure 2. Minimum energy adsorption structures of Pt_n ($n = 1-8$) clusters on the partially reduced 4×2 rutile (110) surface. Light (dark gray), dark (red), and numbered (pink) colors represent Ti, O, and Pt atoms, respectively. Pt atoms are labeled, and discussions about these atoms are given in the text. Bond lengths between the neighboring atoms in the vicinity of the clusters are given in angstroms. The top views of these small Pt clusters are also presented in the insets.

the experimentally observed position of vacancy induced band gap states. In this work, we have set the U value to 4.5 eV for Ti 3d states.[18]

Reduced Rutile (110) Surface. Figure 1 displays side and top views of this partially reduced surface. Reduction of the surface has been obtained by removal of a 2-fold coordinated bridge O atom (O_{Br}) from the relaxed structure of the defect-free surface, and the emergent structure has been relaxed again. The energy required to remove one bridging oxygen atom from the 4×2 stoichiometric rutile (110) surface to form the partially reduced surface is called the vacancy formation energy E_{vf}, and it can be calculated using

$$E_{vf} = E_T[TiO_2(reduced)] + \frac{1}{2}E_T[O_2]$$
$$- E_T[TiO_2(stoic)]$$

Here, $E_T[TiO_2(reduced)]$ and $E_T[TiO_2(stoic)]$ are the total energies of the reduced and stoichiometric surfaces, respec-

tively. In the calculation of E_{vf}, the spin polarized total energy (= −4.90 eV/atom) of the gas phase O_2 molecule has been used, and O_2 has a triplet ground state since the reduced surface has a ferromagnetic ground state with a magnetic moment of 2 μ_B. The calculated E_{vf} is 3.21 eV. The corresponding E_{vf} from GGA+U calculation is 3.40 eV. This 0.19 eV difference between the GGA and GGA+U calculated E_{vf} values might be due to the energy difference between localized and delocalized solutions of excess charges in the reduced surface as a result of oxygen vacancy formation. It is known that the value of E_{vf} depends on the thickness of the slab, the number of fixed layers, and the size of the surface (or distance between the vacancy and its periodic image).[6,34,51−53] For example, E_{vf} becomes 3.74 eV for the fully relaxed slab model calculated by using GGA. Similarly, E_{vf} has been calculated as 3.6 eV for a 4×2 four-layer slab having one fixed bottom layer in ref 7. These results show that the formation energy considerably depends on the slab models and increases with decreasing number of frozen layers within

the model. Introducing an O vacancy induces significant structural modifications on the ideal defect-free rutile surface. The creation of the O vacancy causes both inward (along the [110] direction by ~0.25 Å) and lateral (along the [001] direction by ~0.2 Å) movement of neighboring under-coordinated Ti atoms to increase their coordinations. The O vacancy density or concentration for this 4 × 2 surface is 1/8 (or 12.5%), and separation of defects is about 12 Å in our calculations.

Adsorption of Pt_n ($n = 1–8$) Clusters on the Reduced Rutile (110) Surface. *Pt_1 Case.* We have first investigated the binding of a Pt atom on the partially reduced surface. A surface supercell of 4 × 2 has been used in all calculations to prevent the interaction between the adjoint clusters. Various possible adsorption sites have been searched not only for Pt monomer but also for larger Pt clusters to find the energetically most stable adsorption sites. The effects of spin polarization on calculations have been tested and found to be negligible for the final atomic structures and energetics. To investigate the clustering ability and energetics, we have defined a cohesive energy as

$$E_{coh} = (E_T[TiO_2] + nE_T[Pt] - E_T[TiO_2-Pt_n])/n$$

for the adsorbed Pt_n clusters. In this formula, $E_T[TiO_2]$, $E_T[Pt]$, and $E_T[TiO_2-Pt_n]$ are the total energies of a partially reduced 4 × 2 slab having a single O vacancy, free Pt atom, and fully relaxed TiO_2-Pt_n system, respectively. Here, n represents the number of Pt atoms adsorbed on the surface. The surface oxygen vacancy site has been found to be the energetically most stable adsorption site for a single Pt atom with an adsorption energy of 3.16 eV, shown in Figure 2(a). The Pt atom binds directly to the two Ti atoms neighboring the vacancy with an average interatomic distance of 2.38 Å. Due to the filling of the oxygen vacancy site by the Pt atom, the distance between these Ti atoms increases, and the structure of the surface relaxes back, similar to the one of the defect-free surface.

Pt_2 Case. The Pt_2 cluster has been constructed by adding a single Pt (which is labeled as Pt2) atom to the Pt_1–surface system and allowing the structure to relax again. The second Pt atom prefers to bind to the previously adsorbed Pt and a 5-fold coordinated Ti atom (Ti_{5c}). Pt1–Pt2 and Pt2–Ti_{5c} bond lengths are 2.51 and 2.34 Å, respectively. E_{coh} is 3.38 eV for this Pt dimer case. According to ref 18, both Pt atoms occupy the vacancy site. However, our extensive GGA and GGA+U calculations reveal that our adsorption structure is energetically (about 0.6 eV within GGA+U) more favorable than that of ref 18.

Pt_3 Case. This cluster has been obtained by adding a third Pt atom (Pt3) to the ground state structure of the Pt_2–surface system. Not only Pt_3 but also other clusters ($n > 3$) have been constructed by using the same procedure. The Pt_3 cluster has a triangular ground state structure which lies almost parallel to the surface. Figure 2(c) presents the lowest-lying structure of the Pt_3 clusters adsorbed on the surface. Pt1 and Pt3 atoms of the Pt_3 cluster sit at the vacancy site of the reduced surface. The shortest (longest) Pt–Pt bond length is 2.55 (2.64) Å. Pt atoms at the defect site also bind to the neighboring bridge O atoms with an average interatomic distance of 2.04 Å. E_{coh} increases to 3.66 eV when an extra Pt atom is added to the Pt_2–surface system.

Pt_4 Case. This cluster has Y-shaped structure that consists of a triangular and a linear portion. The subsequently adsorbed Pt atom (Pt4) binds to the bridge O (O_{2c}), the Ti_{5c}, and the Pt2

atom of the Pt_3 cluster. Pt4–O_{2c} and Pt4–Ti_{5c} bond lengths are 2.18 and 2.43 Å, respectively. Pt–Pt interatomic distances range from 2.43 to 2.59 Å. Pt2 and Pt4 bind to the same Ti_{5c} atom which is in the valley between the bridging O rows. This Ti_{5c} atom moves upward as a result of the interaction with the cluster atoms. The interatomic distance between Ti_{5c} and its neighboring bulk 3-coordinated O atom (O_{3c}) increases to 2.54 Å. In this cluster case, E_{coh} is 3.74 eV which is greater than that of $n < 4$ clusters.

Pt_5 Case. Figure 2(e) shows the structure of the Pt_5 cluster which has a side-capped rhombus geometry. The Pt5 atom binds to Pt2, Pt3, Pt4, and a Ti_{5c} atom. Pt5–Pt3 and Pt5–Ti_{5c} bond lengths are 2.72 and 2.46 Å, respectively. This Ti_{5c} atom moves 0.17 Å upward from its equilibrium position. In this cluster case, we have calculated E_{coh} as 3.83 eV.

Pt_6 Case. The top view of the Pt_6 cluster looks like a bridge extended between two bridge oxygen rows. It has a rhomboid geometry and four corner atoms of the Pt_6 cluster bound to both 5-fold coordinated Ti and 2-fold coordinated bridge O atoms. Pt–Pt (Pt–Ti) interatomic distances range from 2.51 (2.50) to 2.67 (2.68) Å. E_{coh} becomes 3.85 eV upon adsorption of the Pt6 atom.

Pt_7 Case. The lowest-lying structure of the Pt_7 cluster displayed in Figure 2(g) has a three-dimensional (3D) structure whose Pt7 atom only binds to cluster atoms (Pt2, Pt4, Pt5, and Pt6) with interatomic distances of 2.90, 2.53, 2.77, and 2.57 Å, respectively. This three-dimensional structure with E_{coh} of 3.90 eV is energetically 0.03 eV more favorable than its planar isomer, from the comparison by using $E_{coh}(3D) - E_{coh}(2D)$. Note that, if we directly use total energies of 3D and 2D structures for comparison, the former one is about 0.19 eV more stable than the latter one. The interatomic distance between Pt_6 (Pt_4) and its nearest Ti_{5c} (Ti_{5c}) increases from 2.64 (2.58) to 3.50 (3.44) Å. These Ti atoms slightly move inward. It is prominent that the energy difference is very small between the isomers of the Pt_7 clusters. Therefore, various isomers might be found simultaneously at finite temperatures.

Pt_8 Case. Figure 2(h) shows top and side views of the energetically most stable structure of the supported Pt_8 cluster. In this cluster, Pt8 is adsorbed on the Pt_7 cluster, and there is no direct interaction between the metal oxide and Pt8 atom. Its structure can be anticipated as a combination of two distorted square pyramids. Adsorption of the Pt8 atom modifies the interatomic distances between Pt1, Pt3, and underlying Ti atoms. For instance, the Pt1–Ti bond length increases from 2.56 to 2.80 Å. As expected, E_{coh} of the Pt_8 cluster is greater than that of Pt_7. The calculated E_{coh} is 3.95 eV. For $n \geq 5$ or planar clusters, adsorption of a Pt atom has relatively local effects on the structural properties of the previously adsorbed cluster. However, effects of both Pt7 and Pt8 adatoms are more pronounced and extensive on both interatomic distances and interaction between the clusters and the surface.

Some insights about the substrate effect on the structure of Pt clusters might result from the comparison of supported and gas phase clusters. Hence, we have also studied the structure of the gas phase Pt_n ($n = 1–8$) clusters. Figure 3 shows the binding energies and structures of these Pt_n clusters. We have taken into account the effect of spin polarization; however, spin–orbit coupling has not been considered in the calculations. Previous calculations[54,55] on the gas phase Pt_n clusters have revealed that clusters prefer to form planar structures for $n < 9$. Therefore, we have mainly considered the planar structures for the gas phase cluster calculations. We have
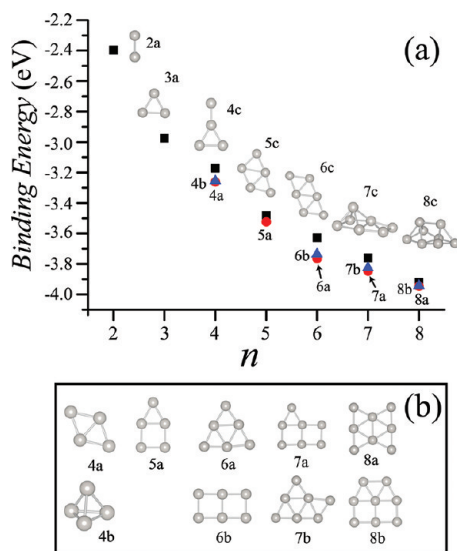
Figure 3. (a) Variation of binding energy of Pt_n clusters in the gas phase as a function of n. The structure of each cluster is shown. Assigned labels are indicated to identify each of the clusters. *na* represents the lowest energy structure which has been considered in this study. Structures of other isomers of Pt_n clusters are presented in (b).

compared the relative stability of the adsorbed clusters (which are labeled as 2a, 3a, 4c, 5c, 6c, 7c, and 8c) and their isomers in the gas phase. Apart from $n \leq 3$, adsorbed clusters do not match with the gas phase ground state structures. This means that the most stable gas phase structure of a particular cluster does not necessarily give the most favorable adsorption configuration on the substrate. We have noticed structural differences between the adsorbed cluster and its gas phase relaxed structure due to the geometrical constraint by the surface structure and the cluster−substrate interaction. For instance, the 4c cluster has a Y-shaped structure. When it is adsorbed on a reduced TiO_2 surface, the linear leg part tilts. Moreover, the bond lengths and angles in adsorbed clusters differ from those of the neutral gas phase geometry. For example, the Pt−Pt bond length in the gas phase Pt_2 dimer elongates from 2.34 to 2.51 Å when adsorbed on the surface.

Energetics. To describe the interaction between the titania surface and Pt clusters in different aspects, we have defined three different energies in addition to E_{coh}. These energies are the binding energy

$$E_{bind} = E_T[TiO_2-Pt_{n-1}] + E_T[Pt] - E_T[TiO_2-Pt_n]$$

the adsorption energy

$$E_{ads} = E_T[TiO_2] + E_T[Pt_n] - E_T[TiO_2-Pt_n])$$

and the second difference in total energies

$$\Delta^2 E = E_T[TiO_2-Pt_{n-1}] + E_T[TiO_2-Pt_{n+1}] - 2E_T[TiO_2-Pt_n]$$

Here, $E_T[TiO_2]$, $E_T[Pt_n]$, and $E_T[TiO_2-Pt_n]$ are the total energies of the bare TiO_2 substrate, the relaxed free Pt_n cluster in the gas phase, and the TiO_2 substrate with the Pt_n cluster, respectively. For the gas phase clusters, we have considered the same structures of the adsorbed clusters. Note that $n > 1$ for the calculation of E_{ads} and $\Delta^2 E$. Therefore, E_{bind} gives the adsorption energy of the nth Pt adatom on the TiO_2-Pt_{n-1}

system. E_{ads} represents the interaction between the Pt clusters and titania surface. Finally, $\Delta^2 E$ reflects the relative stability of a particular Pt_n cluster with respect to its neighbors (Pt_{n-1} and Pt_{n+1}). In the definition of $\Delta^2 E$, $E_T[TiO_2-Pt_{n-1}]$ and $E_T[TiO_2-Pt_{n+1}]$ are the total energies of Pt_{n-1} and Pt_{n+1} clusters adsorbed on the TiO_2 surface, respectively. All these energies have different meanings. For instance, E_{coh} is the average adsorption energy per atom and reflects the clustering ability of Pt atoms on the $TiO_2(110)$ surface, while E_{ads} represents the adsorption energy of the whole cluster. Furthermore, E_{coh} provides a measure of the relative stability for Pt_2 or larger clusters with respect to a single Pt atom.

Figure 4 displays the variation of the cohesive energy (E_{coh}), the binding energy (E_{bind}), the adsorption energy (E_{ads}), and
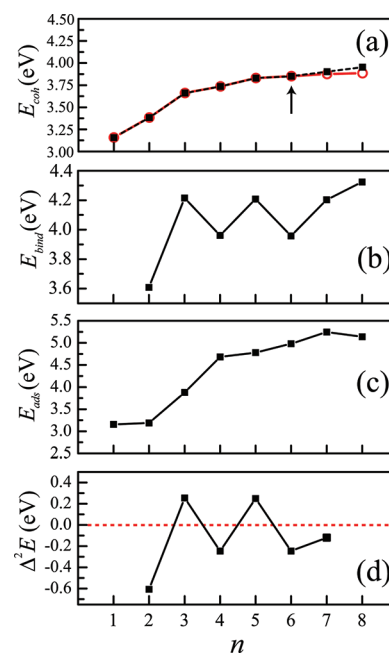

Figure 4. (a) Variation of the clustering or cohesive energy per Pt atom (E_{coh}) with the size of the cluster. Black solid squares and empty red circles represent E_{coh} of the lowest lying structures and their two-dimensional isomers, respectively. Arrow marks the transition point from two- to three-dimensional structures. We have showed the binding energy (E_{bind}) in (b), the adsorption energy (E_{ads}) in (c), and the second difference ($\Delta^2 E$) in total energies in (d). The definitions and physical meanings of these energies are provided in the text.

the second difference in total energies ($\Delta^2 E$) as a function of cluster size. E_{coh} increases with the size of the clusters due to formation of strong Pt−Pt bonds which stabilize the adsorption system. E_{coh} shows small humps at $n = 3$ and 5, which represent the stability of these clusters. When we add a Pt atom away from the vacancy site to the lowest-lying structure of the Pt_2−surface system to form a Pt_3 cluster, the energy difference (ΔE) between the ground state structure of Pt_3−surface and this adsorption mode becomes 0.78 eV. Similarly, ΔE is 0.27 eV for the Pt_4 cluster, and it is 0.61 eV for the Pt_6 cluster. Therefore, each adsorbed Pt atom prefers to bind to the previously formed Pt cluster. As a result, the vacancy site can be considered as a nucleation center for the growth of Pt clusters on the partially reduced rutile (110) surface. Planar structures are favorable up to $n = 6$. This growth behavior suggests that Pt−TiO_2 interaction is the main driving force for the early stages of Pt cluster growth over the rutile surface. E_{coh} for planar clusters

approaches to a constant value after $n = 5$ as depicted in Figure 4(a). Due to the structural transition from 2D to 3D, we have observed a sharp increase in E_{coh} when a Pt atom is added to the Pt_6–TiO_2 system. We have examined both 2D and 3D clusters in this work. For the $n = 4$ cluster, the energy difference between the ground state adsorption mode which adopts a planar geometry and its 3D isomer having tetrahedron structure is 0.32 eV. This difference is 0.19 and 0.56 eV for $n = 7$ and $n = 8$ clusters, respectively. Note that these numbers are total energy differences but not the E_{coh} differences. According to a recent experimental study,[56] Pt_n clusters smaller than Pt_7 have planar structures, whereas those larger than Pt_8 prefer to form 3D structures. If one considers the very small energy differences between 2D and 3D isomers of $n = 7$ and 8 clusters and finite temperature effects, our results, in spite of the controversy at the 2D to 3D transition point, very well agree with the experimental results.[56]

The energy gain or E_{bind} upon addition of an extra Pt atom to the clusters has been calculated to get more insight into the growth of Pt clusters and to provide an understanding for the relative stabilities of these clusters. With the exception of $n = 8$, we have observed even−odd oscillations between $n = 2$ and $n = 7$ for E_{bind} as shown in Figure 4(b). It was previously mentioned that 3D structures are energetically favorable for $n > 6$. This deviation of E_{bind} of the $n = 8$ cluster from clear even−odd oscillation could be an indication of the transition toward 3D structures. After $n = 6$, Pt−Pt interaction starts to dominate the growth behavior of the Pt clusters.

We have also considered the interaction between the titania surface and the Pt cluster as a whole. Figure 4(c) shows the variation of E_{ads} as a function of n. Notice that E_{coh}, E_{bind}, and E_{ads} values are equal for the Pt_1–TiO_2 system. Then, E_{ads} increases up to $n = 7$. From the calculated E_{ads} values, one can easily argue that all clusters strongly interact with the titania substrate. E_{ads} is found to be 3.16 eV for the Pt monomer and becomes 5.15 eV in the case of $n = 7$. The substantial stretch of bond lengths between the Pt atoms of isolated clusters when adsorbing on the surface also proves the strong interaction between the substrate and the supported cluster. For instance, the Pt−Pt interatomic distance in Pt_2 (Pt_3) increases from 2.34 (2.49) to 2.51 (2.55 and 2.64) Å. It is well-known that oxide surface−metal cluster interaction influences greatly the catalytic activity of the supported metal cluster. In this study, we have tried to find out the most favorable adsorption structures for Pt_n clusters. For this reason, we have energetically compared the different adsorption modes based on total energy calculations. However, in reality, free energy is the most important physical quantity, and the cluster−surface system may not be at equilibrium. Therefore, metastable structures might be formed thermodynamically on the surface. The other important point is the vacancy concentration which also influences reactivity of these defect sites, growth of metal clusters, and interfacial properties between the surface and supported metal cluster. In this study, we have examined the reduced surface which has low vacancy concentration. In fact, the formation of a second vacancy nearby the existant one (vacancy pair) or larger vacancy clusters is energetically unfavorable compared to isolated vacancies, which is due to short-range repulsive interactions between vacancies on a given bridge oxygen row.[57] Experimentally, scanning tunneling microscope measurements have indicated that oxygen vacancies prefer to remain isolated.[58]

Additional information about the growth of the Pt_n clusters on the titania surface can be obtained from the calculated second difference in total energies ($\Delta^2 E$) (see Figure 4(d)). $\Delta^2 E$ exhibits an oscillatory behavior. Local maximum peaks of $\Delta^2 E$ have been found at $n = 3$ and 5, indicating that the adsorbed Pt_n clusters with these values of n are more stable than their neighboring clusters. Both $\Delta^2 E$ and E_{bind} verify the strong stability of adsorbed Pt_3 and Pt_5 clusters.

Electronic Structure. Particulary for the description of electronic properties, we have also carried out calculations by using GGA+U in addition to the ones with the GGA functional to make comparison between the two different functionals. It is well-known that local density approximation and all commonly used GGA functionals (such as PW91 or PBE) substantially underestimate the band gap due to the insufficient cancellation of the self-interaction energy inherent in the DFT functionals based on LDA or GGA. We found the band gap for bulk rutile TiO_2 as 1.90 eV with GGA (PW91), which is in very good agreement with previous DFT calculations,[59] but it is much smaller than the experimental value of 3.03 eV.[60] Even performing the DFT+U calculations, the band gap remains well below its experimental value. For instance, the band gap increases just up to 2.5 eV when $U = 9$ eV in LDA+U calculations.[61] Furthermore, Park et al.[61] found an upper limit to U for Ti 3d states based on the electronic structure of the conduction band. They observed an unphysical overlap between the t_{2g} and e_g states for values of U higher than 7 eV. Here, we have set the value of U to 4.5 eV for Ti 3d states[18] to reproduce fairly the experimentally observed position of vacancy induced band gap states. We found that the band gap for bulk rutile TiO_2 increases to 2.24 eV with this U value. However, our aim here is not to achieve the experimental gap value for rutile TiO_2 by considering various functionals. We have mainly focused on binding energies, adsorption structures (which are mostly well described by GGA), and a general picture of the electronic structure with reasonable accuracy.

As pointed out by Di Valentin et al.,[46] structural relaxation plays a key role in the electron localization in the reduced rutile surface. They have shown that the use of a properly distorted geometry is enough to obtain the local electron trapping on the specific Ti sites even by using the PBE exchange-correlation functional on the electronic structure calculations. On the contrary, density of states calculations on the PBE relaxed geometries by employing a hybrid functional like B3LYP have resulted in that the excess electrons are still delocalized on several Ti atoms. Therefore, the proper structural relaxation is essential to realize a localized solution. Accordingly, we have performed full structural relaxation on all optimized GGA ground state structures by using GGA+U to attain the proper distorted geometry due to the vacancy formation. For the sake of a reliable comparison between the electronic properties of Pt_n–TiO_2 systems calculated via GGA and GGA+U, we released all the frozen atoms in two bottom layers shown in Figure 1 and reoptimized all lowest energy structures with GGA as well. In general, the cluster structures, electronic properties, and the charge transfer between the clusters and oxide surface described within GGA+U might be different than those obtained within GGA. We have checked the reliability of results presented in this work by considering several test systems, namely, Pt_2 (which has a different adsorption geometry than of ref 18), Pt_6, and Pt_7 (which has a 3D structure, in contrast to $n \leq 6$ clusters). Our calculations reveal that there is an agreement between GGA and GGA+U
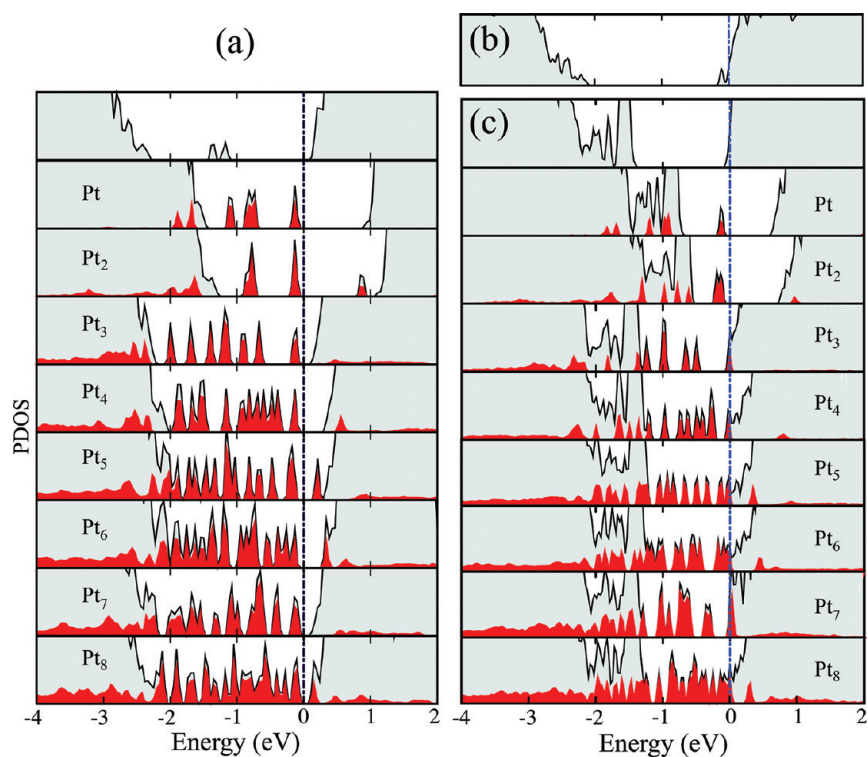
Figure 5. Partial density of states (PDOS) of the Pt_n–surface system. Solid (black) and dark shaded (red) curves represent the total DOS of the Pt_n–TiO_2 system and adsorbed Pt_n clusters, respectively. The Fermi level is shown by a dotted-dashed line. PDOS of Pt_n–TiO_2 systems calculated by using GGA+U are shown in (a). The calculated PDOS of a clean reduced surface with GGA functional is displayed in (b). The electronic properties of Pt_n–TiO_2 from the GGA functional are presented as PDOS in (c) for comparison. Fully relaxed slab models were used in (a) and (b), while the two bottom layers of the slab are fixed in (c).

calculations. Moreover, experimental evidence also verifies that the lowest energy adsorption structures of Pt_n clusters on the reduced TiO_2 surfaces established by using the GGA functional are reliable.[56]

The partial density of states (PDOS) of the bare surfaces and the adsorbed Pt_n clusters and the underlying surfaces are displayed in Figure 5. The zero of the energy corresponds to the Fermi level. As presented in the upper panel of Figure 5(a), the reduced bare surface is semiconducting, and there are two distict peaks about ~1.2 eV below the conduction band (CB) edge within the GGA+U description; in contrast, it is metallic, and the Fermi energy appears around the CB edge according to the GGA (PW91) results (see Figure 5(b)). These outcomes are consistent with the other theoretical works.[18,46] For fully relaxed Pt_n–TiO_2 systems, the outcomes of GGA+U calculations are similar to the ones of standard GGA because Pt atoms occupy the vacancy site, hence only the GGA+U results are presented in Figure 5(a). We have realized that spin polarization is essential to attain correct electronic structure of adsorbed Pt_7 clusters even with GGA+U calculations. We accordingly included the spin polarization for the Pt_7–TiO_2 system; however, only majority spin components are shown in Figure 5 just for complying with the rest of the panels. After all, all the Pt_n adsorbed systems exhibit semiconducting behavior. Adsorption of Pt monomer and dimer reduces the band gap from 2.2 eV, gap of the clean surface, to 0.92 and 1.08 eV, respectively. As a result of this reduction in the effective band gap, optical thresholds of Pt–TiO_2 and Pt_2–TiO_2 systems are lower than that of the clean surface. The visible light photocatalytic activities of Pt-doped TiO_2 have been successfully observed in a recent experiment.[62] Similarly, significant

band gap narrowing occurs upon adsorption of the larger clusters, and Pt atoms bring a number of band gap states depending on the cluster size. These states disperse throughout the band gap of the reduced oxide surface and are known as metal induced gap states.

For further understanding of local structure effects on the electronic structure, we displayed the DOS calculated from slab models with two bottom layers frozen at bulk positions by using GGA in Figure 5(c). First of all, the band gap of the clean reduced surface has been obtained as 1.3 eV (see the uppermost panel in Figure 5(c)), which is much smaller than that of the fully relaxed clean reduced surface. Comparison of the electronic structure of these two slab models reveals that full relaxation of the slab removes stress-driven gap states which are mainly due to the frozen surface atoms. Pt_n–TiO_2 exhibits metallic behavior when $n \geq 3$. The band gap of the surface is filled by energy states arising from cluster atoms, and it disappears, indicating metallization of the Pt–surface system, contrary to the semiconducting nature of the fully relaxed Pt_n–TiO_2 system. In conclusion, fixing some bottom layers hinders the emergence of local structure which results in the localization of excess charge and thereby the semiconducting ground state. Therefore, not only spin polarization (such as the case of adsorbed Pt_7) but also proper structural relaxation are crucial in terms of the electronic structure reduced rutile surface.

The Pt atom has valence electronic structure configuration as s^1d^9. After the adsorption of the Pt atom on the defect site, empty orbitals of the metal atom are filled by excess charge emerged from the O vacancy, and the electronic configuration of Pt becomes s^2d^{10}. As a result, Pt can be theoretically viewed

as a Pt^{2-} anion. This scenario has been both theoretically and experimentally demonstrated for a Au atom adsorbed on the O vacancy of the reduced $TiO_2(110)$ surface.[63] Direct evidence for the charge transfer from the defect sites of the reduced $TiO_2(110)$ surface to the Au atom has been demonstrated in an X-ray photoelectron spectroscopy experiment.[64] Likewise, the DFT-based calculations have been used to elaborate the charging of Au_n clusters on partially reduced rutile surfaces.[23] To elucidate the charge state of adsorbed clusters and the interatomic charge distributions, we have employed Bader charge analysis.[65,66] Bader charges obtained from GGA (GGA +U) charge density calculations imply that 0.65 (0.75) e transfers from the surface to the Pt atom. According to this result, the reduced rutile surface acts as an electron donor. Bader charge on each Pt atom of Pt_n clusters has been calculated within both GGA and GGA+U, and results are tabulated in Table 1. First of all, the charge transfer from reduced oxide surface to Pt_n ($n = 1-3$) clusters was reported previously from Bader charges calculated by using the PBE functional[67] as −0.54 and −0.25 e, respectively, consistent with our GGA results. Briefly, due to the close description of electronic structures, GGA and GGA+U calculations have resulted in similar charge distributions on cluster atoms. In general, there is an agreement between GGA and GGA+U calculations. For example, the sign of net total Bader charge on the Pt_n clusters from both of the calculations is the same; however, there is more charge transfer from the surface to the cluster in GGA+U calculations as revealed from Table 1. The calculated net Bader charges are decreasing with increasing cluster size; for example, it becomes almost zero for the $n = 8$ case in the GGA calculations. It has been proposed that the charge state of the oxide-supported metal clusters plays an important role in catalytic activity of these clusters.[24] To this end, note that Pt2 and Pt5 atoms, which bind to surface 5-fold coordinated Ti (Ti_{5c}) atoms, are always negatively charged. The bond strength between these Ti atoms and their neighboring bulk 3-coordinated O atoms residing just beneath the surface gets weaker upon adsorption of Pt2 and Pt5, which leads to a charge transfer from Ti_{5c} atoms to Pt2 and Pt5. It can also be inferred that binding with the O atom influences the charge state of a particular Pt atom. In general, only Pt2 and Pt5 atoms, which do not directly bind to any O atoms, are always negatively charged. Each adsorbed Pt atom modifies the charge distribution over the previously adsorbed Pt cluster. This argument can be easily inferred from Table 1. We have also found that not only the lowest lying structures of $n \leq 6$ clusters but also planar $n = 7$ and $n = 8$ clusters are negatively charged. As a result, it is expected that a continuous Pt monolayer over the partially or full reduced rutile surface is negatively charged. We can argue that direct contact among the cluster atoms and titania surface is crucial for charge state of the supported metal cluster and amount of transferred charge.

Adsorption of Bimetallic Pt_2Au_m ($m = 1-5$) Clusters on the Reduced Rutile (110) Surface. It has been shown that the Au migration profile on the stoichiometric rutile (110) surface is quite flat relative to Pt.[8] The Au atom can easily diffuse on the stoichiometric surface. Both Pt and Au atoms prefer to bind to the O vacancy site of the reduced surface. However, Au is much more likely to escape from this defect site compared to Pt. These arguments imply the higher sensitivity of catalytic activity of Au on external effects. Au clusters are sintered easily at high temperatures, which leads to not only a loss of surface area but also a loss of catalytic activity. This is an

Table 1. Bader Charge on Each Atom of Pt_n Clusters Calculated from GGA (GGA+U) Charge Density[a]

	Pt	Pt_2	Pt_3	Pt_4	Pt_5	Pt_6	Pt_7	Pt_8
Pt1	−0.65 (−0.75)	−0.35 (−0.42)	−0.04 (−0.15)	−0.02 (−0.10)	−0.02 (−0.10)	0.00 (−0.06)	−0.06 (−0.13)	0.06 (−0.03)
Pt2		−0.22 (−0.27)	−0.29 (−0.37)	−0.21 (−0.27)	−0.16 (−0.20)	−0.12 (−0.15)	−0.18 (−0.13)	−0.15 (−0.19)
Pt3			0.02 (0.00)	0.04 (0.00)	0.05 (0.00)	−0.04 (−0.10)	−0.01 (−0.06)	0.12 (0.10)
Pt4				−0.12 (−0.15)	0.07 (0.05)	0.11 (0.08)	0.25 (0.23)	0.29 (0.29)
Pt5					−0.22 (−0.26)	−0.18 (−0.21)	−0.18 (−0.24)	−0.20 (−0.25)
Pt6						0.00 (−0.04)	0.25 (0.25)	−0.18 (−0.19)
Pt7							−0.14 (−0.15)	−0.11 (−0.11)
Pt8								0.17 (0.17)
ΔQ	−0.65 (−0.75)	−0.57 (−0.69)	−0.31 (−0.53)	−0.31 (−0.51)	−0.28 (−0.51)	−0.23 (−0.49)	−0.06 (−0.32)	0.00 (−0.21)

[a]Total Bader charge ΔQ on the cluster is also given in units of e.

important problem for the nanosized Au catalysis since the size of the supported Au nanoparticles substantially influences the catalytic activity. Note that the desired (or high) activity is obtained for the Au nanoparticles whose diameters are smaller than 5 nm.[2,20,68] Meanwhile, bimetallic Pt−Au clusters offer important advantages for catalysis. First of all, existence of Pt in Pt−Au clusters prevents the sintering of the Au clusters.[69] The oxide-supported metal cluster interaction can be tuned by changing the composition of the Pt−Au bimetallic clusters. Furthermore, Pt−Au clusters can be better catalysts for particular reactions compared to both pure Pt and Au clusters. Pt−Au bimetallic nanoparticles have been used as catalysts for NO reduction,[70] CO oxidation,[71] and CH_3OH oxidation.[72] Therefore, a detailed analysis of bimetallic Pt−Au clusters supported on the oxide surfaces might be very useful.

For these reasons, we have also examined the growth and their structural and electronic properties of bimetallic Pt−Au (Pt_2Au_m, m = 1−5) clusters supported on the reduced titania surface. First, a Pt dimer is adsorbed on a 4 × 2 rutile (110) surface having a single surface oxygen vacancy. Figure 2(b) shows the structure of Pt dimer adsorbed on the vacancy site and underlying substrate. The next step is the growth of Au_m (m = 1−5) clusters on this Pt-loaded surface. Figure 6 displays the lowest-lying structures of Pt−Au bimetallic clusters for each m. As in the case of the Pt_n−surface systems, we have searched the possible spin polarization of the bimetallic clusters as well. However, imposing magnetism on the calculations has altered neither the lowest-lying structures nor the relative energies among the isomers of Pt_2Au, Pt_2Au_2, and Pt_2Au_3 clusters. Henceforth, the results obtained without including the spin polarization will have been presented. The smallest Pt−Au cluster is Pt_2Au_1. In this cluster, the Au atom prefers to sit at the vacancy site which has been already occupied by a Pt atom (which is Pt1). The adsorbed Au atom pushes this Pt atom toward a bridge O atom, and the resulting cluster has a triangular geometry which lies almost parallel to the oxide surface. Interatomic distances of Au−Ti, Au−Pt1, Au−Pt2, and Au−O_{2c} are 2.88, 2.62, 2.68, and 2.20 Å, respectively. Similar to the Pt_n−TiO_2 system, we have studied the energetics of cluster growth to understand the cluster formations in depth. The cohesive or clustering energy per Au atom (E_{coh}) has been defined as

$$E_{coh} = (E_T[TiO_2-Pt_2] + mE[Au]$$
$$- E_T[TiO_2-Pt_2-Au_m])/m$$

for the adsorbed Pt_2Au_m clusters. In this formula, $E_T[TiO_2-Pt_2]$ and $E_T[TiO_2-Pt_2-Au_m]$ are the total energies of the TiO_2-Pt_2 and $TiO_2-Pt_2-Au_m$ systems. E_{coh} is obtained as 2.55 eV for the m = 1 case, while it is calculated as 1.62 eV for the binding of a single Au atom on the partially reduced 4 × 2 rutile (110) surface. This result suggests that there is a significant enhancement of the binding of the Au atom on the reduced surface due to the presence of a Pt dimer on that surface. The Pt_2Au_2 cluster has a planar geometry which is similar to the lowest-lying structure of the supported Pt_4 cluster. The Au2 atom interacts more strongly with the Pt2 atom compared to the interaction between Au2 and neighboring Ti_{5c} as well as the bridge O_{2c} atom. Au2−Pt2, Au2−Ti_{5c}, and Au2−O_{2c} interatomic distances are 2.52, 2.86, and 2.39 Å, respectively. E_{coh} of the Au_2 dimer adsorbed on the reduced surface is 1.82 eV which is about 0.66 eV lower than that of Au_2 dimer absorption on the Pt_2−TiO_2 surface. 3D structures become
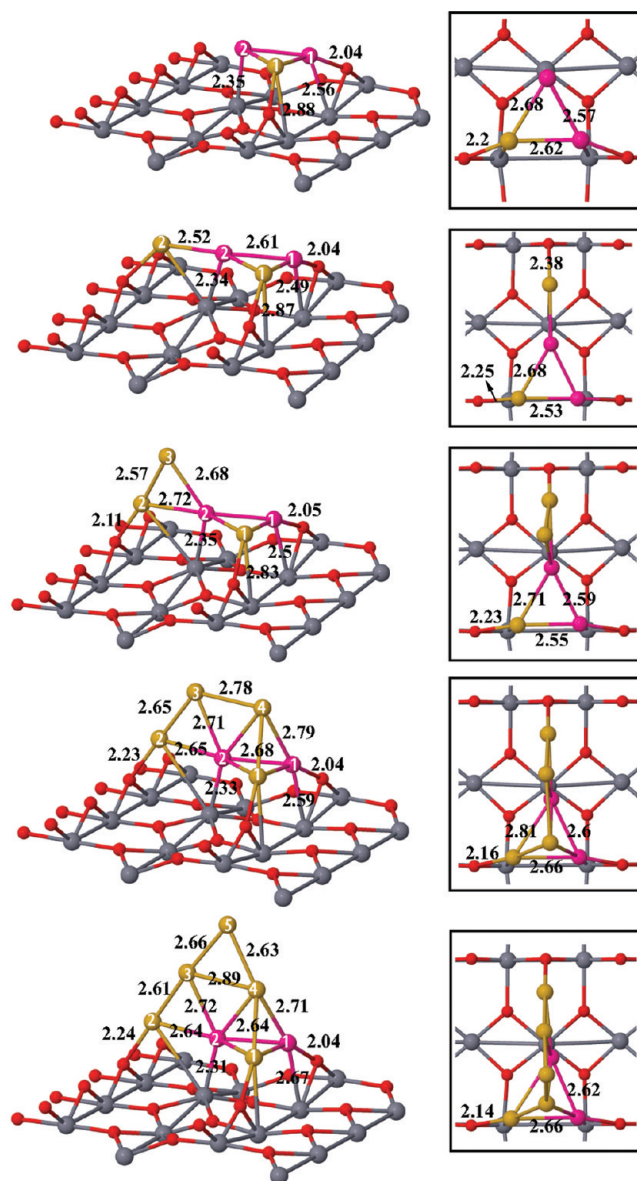

Figure 6. Energetically most stable adsorption structures of Pt_2Au_m (m = 1−5) bimetallic clusters on the partially reduced 4 × 2 rutile (110) surface. The top views are also presented in the right panels. Dark gray, red, pink, and yellow colors represent Ti, O, Pt, and Au atoms, respectively. Some of the bond lengths are shown in angstroms. Pt and Au atoms are labeled, and discussions about these atoms are given in the text.

energetically more stable for $m \geq 3$, and Pt−Au bimetallic clusters tend to grow along the [110] direction. E_{coh} stays almost constant between m = 2 and 4 values. It is largest for both Pt_2Au and Pt_2Au_5 clusters and is evaluated as 2.56 eV. Several optimized structural parameters, calculated E_{coh}'s, the binding energies (E_{bind}), and the second differences in total energies ($\Delta^2 E$) are presented in Table 2. We have used the previous definitions of E_{bind} and $\Delta^2 E$. In the Au dimer and fcc bulk, Au−Au interatomic distances are 2.53 and 2.88 Å, respectively. It is noticed that average Au−Au bond lengths in Pt−Au bimetallic clusters are between those of the dimer and bulk, which is a result of the different coordination number of Au atoms in these three different structures. Au clusters prefer to grow over the previously adsorbed Pt dimer which behaves

5743

dx.doi.org/10.1021/jp2109253 | J. Phys. Chem. C 2012, 116, 5735−5746

Table 2. Bader Charge (Q) on Corresponding Atoms As Well As Total Charge ΔQ (in Units of e) on the Bimetallic Pt_2Au_m Clusters[a]

	Pt_2Au	Pt_2Au_2	Pt_2Au_3	Pt_2Au_4	Pt_2Au_5
Q_{Pt1}	−0.01	−0.09	−0.06	−0.10	0.00
Q_{Pt2}	−0.28	−0.35	−0.31	−0.32	−0.29
Q_{Au1}	0.08	−0.04	0.02	0.07	0.12
Q_{Au2}		−0.09	0.26	0.13	0.14
Q_{Au3}			−0.04	−0.04	0.00
Q_{Au4}				−0.14	0.02
Q_{Au5}					−0.09
ΔQ	−0.06	−0.57	−0.13	−0.40	−0.10
E_{coh}	2.56	2.46	2.46	2.45	2.56
E_{bind}	2.55	2.36	2.46	2.42	3.00
E_{bind}^{gas}	2.16	2.40	2.27	2.34	2.88
$\Delta^2 E$		−0.01	0.05	−0.58	

[a]Cohesive energies (E_{coh}) per Au atom, binding energies E_{bind}, and E_{bind}^{gas} for supported and gas phase clusters, respectively, and second differences in total energies ($\Delta^2 E$) are also listed in eV.

as a nucleation center for the growth of Au clusters. Due to strong interaction between Au and platinized surface compared to interaction between Au and clean or reduced surfaces, Au clusters are prevented from sintering which leads to the reduction of catalytic activities of the nanosized Au particles. From Table 2 and Figure 4(b), it is apparently seen that E_{bind} of Au atoms is smaller than that of Pt atoms. This is a clear indication of stronger interaction of Pt clusters with titania surfaces compared to Au clusters. E_{bind} consists of three interactions which are: (i) Pt dimer−Au, (ii) Au−Au, and (iii) substrate−Au interaction. Except Pt_2Au_5, a maximum change in E_{bind} between the consecutive clusters is about 0.1 eV. From this result and growth behavior of Au clusters, we can infer that the first two interactions dominate E_{bind}. To elucidate the driving force behind the growth of Au clusters on the Pt_2−TiO_2 surface, gas phase energies and structures of Pt_2Au_m clusters have been investigated. For this purpose, we have defined the following energy

$$E_{bind}^{gas} = E_T^{gas}[Pt_2Au_m] - E_T^{gas}[Pt_2Au_{m-1}] - E_T[Au]$$

where $E_T^{gas}[Pt_2Au_m]$ and $E_T^{gas}[Pt_2Au_{m-1}]$ are the total energies of fully relaxed Pt_2Au_{m-1} and Pt_2Au_m clusters in the gas phase. $E_T[Au]$ is the total energy of the free Au atom. E_{bind}^{gas} and E_{bind} have similar meanings. However, the former one reflects the adsorption energy of the mth Au atom to the isolated or gas phase relaxed structure of the Pt_2Au_{m-1} cluster which has almost the same structure as its supported case one. First, we have calculated the binding energy of a single Au to the gas phase Pt dimer as 2.16 eV by considering the atomic energies as a reference, while it is found as 2.55 eV for the supported Pt_2. Therefore, one can easily conclude that a single Au atom mainly binds to the surface via a Pt dimer. Similarly, E_{bind}^{gas} has been obtained for other clusters and tabulated in Table 2. In some cases, E_{bind}^{gas} is greater than E_{bind}, which is due to structural differences and relaxation effects present in gas phase clusters. The Pt_2Au_4 cluster is highly unstable in the gas phase. We have obtained a 2D structure upon structural relaxation. For the E_{bind}^{gas} calculation, the Pt_2Au_4 structure constrained to the supported case one has been used. This explains the relatively higher stability of Pt_2Au_5 with respect to other structures. Table 2 also shows the computed $\Delta^2 E$ values which indicate the strong stability of Pt_2Au_3 relative to its neighbors.

We have also calculated the Bader charge on each atom and total Bader charge for all supported Pt−Au clusters (see Table 2). Similar to adsorbed Pt_n clusters, all bimetallic clusters considered here are negatively charged. Pt1 and Au3 atoms exchange a small amount of charge with other Au and Pt atoms and the oxide surface compared to Pt2 and Au1. Pt2 atom is always negatively charged as in the case of Pt_n clusters. Adsorption of a gold atom on the Pt_2−surface system drastically changes the total charge on the Pt1 atom which is negatively charged in the pure Pt_2 cluster adsorbed on the reduced surface. The charge transfer between the Au and Pt atoms adds a new degree of freedom to get a better catalyst. By playing with composition, size, and structure of Pt−Au bimetallic clusters, one can tune electronic properties as well as charge transfer between Au and Pt atoms. The density of states calculations (not shown) for bimetallic clusters have also been performed. We found that bimetallic clusters exhibit semiconducting behavior and introduce gap localized states originating from the Pt and Au atoms in the surface band gap similar to the Pt_n clusters.

CONCLUSION

We have examined the growth, energetics and structural and electronic properties of small Pt_n ($n = 1−8$) and bimetallic Pt_2Au_m ($m = 1−5$) clusters, supported on the 4×2 rutile (110) surface having single oxygen vacancy. We found that the vacancy site behaves as a nucleation center for the growth of Pt clusters. In the case of the Pt monomer, the Pt atom preferentially binds to the O vacancy site. Clusters tend to grow around this Pt monomer. For $n = 1−6$, Pt clusters prefer to form planar or 2D structures. We have also observed that the strong Pt cluster−TiO_2 interaction is responsible for the 2D growth of Pt clusters when the coverage is low. After $n = 7$, formation or growth of 3D clusters becomes energetically favorable. The clustering or cohesive energy per Pt atom (E_{coh}) of Pt_n clusters adsorbed on the partially reduced rutile (110) surface increases as the size of the clusters grows. For electronic properties, we have performed both GGA and GGA+U calculations which essentially result in the same electronic structures for all Pt_n−TiO_2 systems. The adsorption of Pt_n clusters brings a number of band gap states depending on the size of the cluster, leading to significant band gap narrowing. Charge transfer among the cluster atoms and underlying oxide surface is more pronounced for Pt_n clusters. For the bimetallic PtAu cluster case, Au clusters have been grown on the Pt_2−surface system. The Pt dimer has been previously adsorbed at the vacancy site. Au clusters have been nucleated around this Pt dimer which enhances the binding of Au atoms to the oxide surface. The variation of E_{coh} for Pt−Au clusters is almost constant and lower than that of Pt clusters. Our findings clearly demonstrate that the presence of oxygen vacancy and preadsorbed Pt dimer on the TiO_2 surface significantly alters the adsorption and limits the diffusion of Au atoms.

AUTHOR INFORMATION

Corresponding Author
*E-mail: gulseren@fen.bilkent.edu.tr.

Present Address
[†]Faculty of Science and Technology and MESA+ Institute for Nanotechnology, University of Twente, P.O. Box 217, 7500 AE Enschede, The Netherlands.

REFERENCES

(1) Diebold, U. *Surf. Sci. Rep.* **2003**, *48*, 53−229.

(2) Valden, M.; Lai, X.; Goodman, D. W. *Science* **1998**, *281*, 1647−1650.

(3) Kowalska, E.; Remita, H.; Colbeau-Justin, C.; Hupka, J.; Belloni, J. *J. Phys. Chem. C* **2008**, *112*, 1124−1131.

(4) Han, Y.; Liu, C. J.; Ge, Q. F. *J. Phys. Chem. B* **2006**, *110*, 7463−7472.

(5) Vittadini, A.; Selloni, A. *J. Chem. Phys.* **2002**, *117*, 353−361.

(6) Vijay, A.; Mills, G.; Metiu, H. *J. Chem. Phys.* **2003**, *118*, 6536−6551.

(7) Chrétien, S.; Metiu, H. *J. Chem. Phys.* **2007**, *127*, 084704. Chrétien, S.; Metiu, H. *J. Chem. Phys.* **2007**, *127*, 244708.

(8) Iddir, H.; Öğüt, S.; Browning, N. D.; Disko, M. M. *Phys. Rev. B* **2005**, *72*, 081407.

(9) Pillay, D.; Hwang, G. S. *Phys. Rev. B* **2005**, *72*, 205422.

(10) Iddir, H.; Skavysh, V.; Öğüt, S.; Browning, N. D.; Disko, M. M. *Phys. Rev. B* **2006**, *73*, 041403.

(11) Gong, X.-Q.; Selloni, A.; Dulub, O.; Jacobson, P.; Diebold, U. *J. Am. Chem. Soc.* **2008**, *130*, 370−381.

(12) Mete, E.; Uner, D.; Gülseren, O.; Ellialtoglu, Ş. *Phys. Rev. B* **2009**, *79*, 125418.

(13) Mete, E.; Gülseren, O.; Ellialtoğlu, Ş *Phys. Rev. B* **2009**, *80*, 035422.

(14) Marri, I.; Ossicini, S. *Solid State Commun.* **2008**, *147*, 205−207.

(15) Pabisiak, T.; Kiejna, A. *Phys. Rev. B* **2009**, *79*, 085411.

(16) Matthey, D.; Wang, J. G.; Wendt, S.; Matthiesen, J.; Schaub, R.; Lagsgaard, E.; Hammer, B.; Besenbacher, F. *Science* **2007**, *315*, 1692−1696.

(17) Shibata, N.; Goto, A.; Matsunaga, K.; Mizoguchi, T.; Findlay, S. D.; Yamamoto, T.; Ikuhara, Y. *Phys. Rev. Lett.* **2009**, *102*, 136105.

(18) Çelik, V.; Ünal, H.; Mete, E.; Ellialtoglu, S. *Phys. Rev. B* **2010**, *82*, 205113.

(19) Haruta, M.; Yamada, N.; Kobayashi, T.; Iijima, S. *J. Catal.* **1989**, *115*, 301−309.

(20) Bamwenda, G. R.; Tsubota, S.; Nakamura, T.; Haruta, M. *Catal. Lett.* **1997**, *44*, 83−87.

(21) Chen, M. S.; Goodman, D. W. *Science* **2004**, *306*, 252−255.

(22) Tauster, S. J.; Fung, S. C.; Garten, R. L. *J. Am. Chem. Soc.* **1978**, *100*, 170−175.

(23) Chrétien, S.; Metiu, H. *J. Chem. Phys.* **2006**, *126*, 104701.

(24) Wang, J. G.; Hammer, B. *Top. Catal* **2007**, *44*, 49−56.

(25) Chung, H. J.; Yurtsever, A.; Sugimoto, Y.; Abe, M.; Morita, S. *Appl. Phys. Lett.* **2011**, *99*, 123102.

(26) Payne, M. C.; Teter, M. P.; Allen, D. C.; Arias, T. A.; Joannopoulos, J. D. *Rev. Mod. Phys.* **1992**, *64*, 1045−1097.

(27) Numerical computations have been carried out by using VASP software: Kresse, G.; Hafner, J. *Phys Rev B* **1993**, *47*, 558−561. Kresse, G.; Furthmüller, J. *Phys Rev B* **1996**, *54*, 11169−11186.

(28) Kohn, W.; Sham, L. J. *Phys. Rev.* **1965**, *140*, A1133−A1138. Hohenberg, P.; Kohn, W. *Phys. Rev.* **1964**, *136*, B864−B871.

(29) Blöchl, P. E. *Phys. Rev. B* **1994**, *50*, 17953−17979.

(30) Kresse, G.; Joubert, D. *Phys. Rev. B* **1999**, *59*, 1758−1775.

(31) Perdew, J. P.; Chevary, J. A.; Vosko, S. H.; Jackson, K. A.; Pederson, M. R.; Singh, D. J.; Fiolhais, C. *Phys. Rev. B* **1992**, *46*, 6671−6687.

(32) Methfessel, M.; Paxton, A. T. *Phys. Rev. B* **1989**, *40*, 3616−3621.

(33) Monkhorst, H. J.; Pack, J. D. *Phys. Rev. B* **1976**, *13*, 5188−5192.

(34) Hameeuw, K. J.; Cantele, G.; Ninno, D.; Trani, F.; Iadonisi, G. *J. Chem. Phys.* **2006**, *124*, 024708.

(35) Kiejna, A.; Pabisiak, T.; Gao, S. W. *J. Phys.: Condens. Matter.* **2006**, *18*, 4207−4217.

(36) Busayaporn, W.; Torrelles, X.; Wander, A.; Tomic, S.; Ernst, A.; Montanari, B.; Harrison, N. M.; Bikondoa, O.; Joumard, L.; Zegenhagen, J.; Cabailh, G.; Thornton, G.; Lindsay, R. *Phys. Rev. B* **2010**, *81*, 153404.

(37) Abrahams, S. C.; Bernstein, J. L. *J. Chem. Phys.* **1971**, *55*, 3206−3211.

(38) Burdett, J. K.; Hughbanks, T.; Miller, G. J.; Richardson, J. W. Jr.; Smith, J. V. *J. Am. Chem. Soc.* **1987**, *109*, 3639−3646.

(39) Howard, C. J.; Sabine, T. M.; Dickson, F. *Acta Crystallogr. Sect. B: Struct. Sci.* **1991**, *47*, 462−468.

(40) Krüger, P.; Bourgeois, S.; Domenichini, B.; Magnan, H.; Chandesris, D.; Le Fvre, P.; Flank, A. M.; Jupille, J.; Floreano, L.; Cossaro, A.; Verdini, A.; Morgante, A. *Phys. Rev. Lett.* **2008**, *100*, 055501.

(41) Pirovano, M. V. G.; Hofmann, A.; Sauer, J. *Surf. Sci. Rep.* **2007**, *62*, 219−270.

(42) Kowalski, P. M.; Camellone, M. F.; Nair, N. N.; Meyer, B.; Marx, D. *Phys. Rev. Lett.* **2010**, *105*, 146405.

(43) Deskins, N. A.; Dupuis, M. *Phys. Rev. B* **2007**, *75*, 195212.

(44) Deskins, N. A.; Rousseau, R.; Dupuis, M. *J. Phys. Chem. C* **2009**, *113*, 14583−14586.

(45) Deskins, N. A.; Rousseau, R.; Dupuis, M. *J. Phys. Chem. C* **2011**, *115*, 7562−7572.

(46) Di Valentin, C.; Pacchioni, G.; Selloni, A. *Phys. Rev. Lett.* **2006**, *97*, 166803.

(47) Morgan, B. J.; Watson, G. W. *Surf. Sci.* **2007**, *601*, 5034−5041.

(48) Dudarev, S. L.; Botton, G. A.; Savrasov, S. Y.; Humphreys, C. J.; Sutton, A. P. *Phys. Rev. B* **1998**, *57*, 1505−1509.

(49) Chrétien, S.; Metiu, H. *J. Phys. Chem. C* **2011**, *115*, 4696−4705.

(50) Mattioli, G.; Filippone, F.; Alippi, P.; Amore Bonapasta, A. *Phys. Rev. B* **2008**, *78*, 241201.

(51) Oviedo, J.; San Miguel, M. A.; Sanz, J. F. *J. Chem. Phys.* **2004**, *121*, 7427−7433.

(52) Hameeuw, K.; Cantele, G.; Ninno, D.; Trani, F.; Iadonisi, G. *Phys. Status Solidi A* **2006**, *203*, 2219−2222.

(53) Pabisiak, T.; Kiejna, A. *Solid State Commun.* **2007**, *144*, 324−328.

(54) Kumar, V.; Kawazoe, Y. *Phys. Rev. B* **2008**, *77*, 205418.

(55) Bhattacharyya, K.; Majumder, C. *Chem. Phys. Lett.* **2007**, *446*, 374−379.

(56) Isomura, N.; Wu, X.; Watanabe, Y. *J. Chem. Phys.* **2009**, *131*, 164707.

(57) Zhang, Z.; Ge, Q.; Li, S.-C.; Kay, B. D.; White, J. M.; Dohnálek, Z. *Phys. Rev. Lett.* **2007**, *99*, 126105.

(58) Diebold, U.; Lehman, J.; Mahmoud, T.; Kuhn, M.; Leonardelli, G.; Hebenstreit, W.; Schmid, M.; Varga, P. *Surf. Sci.* **1998**, *411*, 137−153.

(59) Çakr, D.; Gülseren, O. *Phys. Rev. B* **2009**, *80*, 125424.

(60) Pascual, J.; Camassel, J.; Mathieu, H. *Phys. Rev. Lett.* **1977**, *39*, 1490−1493; *Phys. Rev. B* **1978**, *18*, 5606−5614.

(61) Park, S.-G.; Magyari-Köpe, B.; Nishi, Y. *Phys. Rev. B* **2010**, *82*, 115109.

(62) Kim, S.; Hwang, S.-J.; Choi, W. *J. Phys. Chem. B* **2005**, *109*, 24260−24267.

(63) Wörz, A. S.; Heiz, U.; Cinquini, F.; Pacchioni, G. *J. Phys. Chem. B* **2005**, *109*, 18418−18426.

(64) Jiang, Z.; Zhang, W.; Jin, L.; Yang, X.; Xu, F.; Zhu, J.; Huang, W. *J. Phys. Chem. C* **2007**, *111*, 12434−12439.

(65) Henkelman, G.; Arnaldsson, A.; Jónsson, H. *Comput. Mater. Sci.* **2006**, *36*, 354−360.

(66) Sanville, E.; Kenny, S. D.; Smith, R.; Henkelman, G. *J. Comput. Chem.* **2007**, *28*, 899−908.

(67) Ammal, S. C.; Heyden, A. *J. Chem. Phys.* **2010**, *133*, 164703.

(68) Lee, S.; Fan, C.; Wu, T.; Anderson, S. L. *J. Am. Chem. Soc.* **2004**, *126*, 5682−5683.

(69) Park, J. B.; Conner, S. F.; Chen, D. A. *J. Phys. Chem. C* **2008**, *112*, 5490−5500.

(70) Mihut, C.; Descorme, C.; Duprez, D.; Amiridis, M. D. *J. Catal.* **2002**, *212*, 125−135.

(71) Chilukuri, S.; Joseph, T.; Malwadkar, S.; Damle, C.; Halligudi, S. B.; Rao, B. S.; Sastry, M.; Ratnasamy, P. *Stud. Surf. Sci. Catal.* **2003**, *146*, 573−576.

(72) Luo, J.; Maye, M. M.; Kariuki, N. N.; Wang, L.; Njoki, P.; Lin, Y.; Schadt, M.; Naslund, H. R.; Zhong, C. J. *Catal. Today* **2005**, *99*, 291−297.

5746

dx.doi.org/10.1021/jp2109253 | *J. Phys. Chem. C* 2012, 116, 5735−5746